ISSN 1027-4510, Journal of Surface Investigation: X-ray, Synchrotron and Neutron Techniques, 2023, Vol. 17, Suppl. 1, pp. S43–S50. © Pleiades Publishing, Ltd., 2023.

Comparison of Properties of the ZrN Mononitride Coating and (Zr + Ti–B–Si–Ni)N Multicomponent Coating Obtained by Vacuum-Arc Plasma-Assisted Deposition

A. A. Leonov[a, *], V. M. Savostikov[a, **], V. V. Denisov[a], Yu. A. Denisova[a], A. B. Skosyrsky[a, b], M. V. Savchuk[a], M. S. Syrtanov[c], A. V. Pirozhkov[c], and A. N. Shmakov[d]

[a] *Institute of High Current Electronics, Siberian Branch, Russian Academy of Sciences, Tomsk, 634055 Russia*

[b] *Tomsk State University, Tomsk, 634050 Russia*

[c] *Tomsk Polytechnic University, Tomsk, 634050 Russia*

[d] *Budker Institute of Nuclear Physics, Siberian Branch, Russian Academy of Sciences, Novosibirsk, 630090 Russia*

**e-mail: laa-91@yandex.ru*

***e-mail: svm.53@mail.ru*

Received April 22, 2023; revised June 26, 2023; accepted June 26, 2023

Abstract—The paper presents the results of comparative study of the mechanical properties and heat resistance of a zirconium nitride mononitride coating and a multicomponent coating obtained by sequential and simultaneous deposition of zirconium and multicomponent cathode (titanium, boron, silicon, and nickel) in a nitrogen-containing medium. Multicomponent cathode was fabricated by self-propagating high-temperature synthesis with simultaneous pressing. The coatings were deposited on the hard alloy VK8 by the vacuum-arc plasma-assisted method. Material science studies of coatings included: measuring the thickness of coatings by calo testing, evaluating the adhesion strength of a coating to a substrate by the Rockwell method and scratch testing, measuring hardness before and after high-temperature annealing in air at a temperature of 700°C for 60 min, X-ray phase analysis of coatings before and after high-temperature annealing. Multicomponent coating (Zr + Ti–B–Si–Ni)N was also investigated for heat resistance in real time by X-ray phase analysis using synchrotron radiation. The adhesive strength of the multicomponent coating (Zr + Ti–B–Si–Ni)N satisfies the generally accepted quality requirements for vacuum-arc coatings. The residual hardness of the multicomponent coating (Zr + Ti–B–Si–Ni)N after high-temperature annealing significantly and noticeably exceeds the hardness of the ZrN coating after annealing. Data of X-ray phase analysis confirm the high heat resistance of the multicomponent coating (Zr + Ti–B–Si–Ni)N, which, together with the results of mechanical tests, allows us to conclude that it is promising for practical purposes.

Keywords: mechanical properties, heat resistance, nitride coating, multicomponent cathode, self-propagating high-temperature synthesis, vacuum-arc plasma-assisted deposition method, adhesion strength, hardness, X-ray phase analysis, synchrotron radiation

DOI: 10.1134/S1027451023070315

INTRODUCTION

The earliest types of protective and hardening coatings applied on tools and machine parts were coatings made of titanium nitride (TiN) [1–3] and zirconium nitride (ZrN) [4–6]. However, over time, the physical and mechanical properties of these mononitride coatings ceased to meet the requirements of industrial applications [7]. This stemmed from intensification of machining and automation of technological processes, as well as from more diversified and severe operating conditions of machine parts. Therefore, new coatings were required which would withstand significantly increased thermomechanical loads on the cutting edges of tools, have guaranteed lifetimes to prevent the stop of an automated cycle, and resist to various types of wear. Thus, the challenge was to ensure a quite high resistance to a complex of destructive factors that may act on the working surfaces of workpieces. This involved the requirement that the physical and mechanical properties of the coatings should be suited to specific operating conditions. It is obvious that such a problem can be solved with the use of multilayer and multicomponent coatings with each of the layers having certain physicomechanical and functional properties. This can be achieved by using plasma-ion methods that provide the most promising technological way of coating deposition due to their diversified capabilities and environmental friendliness.

The properties of base nitride compounds can be improved by alloying them with additional elements.

For example, it was shown [8] that adding a second alloying element to the composition of plasma-ion $TiMe_1N$ coatings (where Me_1 is the first alloying element) improved additionally the physical and mechanical properties of the coatings and, as a result, the working capacity of the cutting tools having this type of coating. The resulting nitrides of a $TiMe_1Me_2N$ composition have a complex structure, which, according to the authors of [8], is associated with the formation of coating microlayers from plasma flows containing a variety of chemical species. It was found [9] that a common feature of complex composition coatings is an increased half-width of the X-ray diffraction line, indicating an increased density of lattice microdistortions and defects. Changes in the coating structural parameters lead to an increase in residual compressive stresses, elastic modulus, and yield strength. Using TiZrN coatings as an example, the authors of [9] revealed that adding a third nitride-forming element (in particular, Si) to the coating composition additionally changed the coating structural parameters and improves its physical and mechanical properties. Thus, the hardness of the TiZrSiN coatings achieved 44.38 GPa, i.e., it increased by factors of 1.21 and 1.59 compared to TiZrN and TiN coatings, respectively. These changes substantially improved the performance of cutting tools with TiZrSiN coatings compared to TiN mononitride coatings. The wear rate of the cutting tools with TiZrSiN coatings was by factors of 1.82 and 3.04 lower compared to those with TiZrN and TiN coatings, respectively, while for the cutting tools with TiZrN coatings it was lower only by a factor of 1.67 compared to those with TiN coatings [9].

The efficiency of multi-element coatings using boron and silicon as the additional alloying element was confirmed in [10, 11]. In the vacuum-arc synthesis of test coatings, cathodes fabricated by self-propagating high-temperature synthesis (SHS) were used. The composition of these cathodes initially included the second (boron) and third (silicon) elements in addition to titanium used as the base element. The field tests of tools with these coatings showed their high efficiency. For the (Ti–B–Si)N-coated tools, all measured parameters (wear on the front and back surfaces of the cutters and the roughness of the machined surface) were several times greater compared to the tools with conventional TiN coatings [11]. In our previous study [12], we used similar coatings of composition (Ti–B–Si–Ni)N that were deposited on VK-8 tool hard alloy by vacuum-arc deposition of SHS cathodes. It was found that coatings of this type have a high hardness (about 41 GPa), due to the presence of titanium borides in its composition. However, the Rockwell method and scratch testing revealed that the coating is characterized by a stressed state and insufficient adhesion to the substrate. As a result, this coating does not withstand high temperatures. In particular, it completely peeled off after being heated in air to 700°C.

In [13] the requirements that should be placed on industrial tool coatings are formulated. The main of them are the following: the coating should exhibit a proper adhesion strength to the tool, high hardness, sufficient heat resistance. Therefore, there is a challenge of selecting a proper material for the binding sublayer to ensure the multi-element hard coating performance under shock loads. In addition, the cutting edges of tools inevitably suffer from local thermal effects. Therefore, it is necessary to ensure proper thermal stability of the coatings.

To extend our previous study [12], we aimed at developing and investigating such a variant of the coating, which would also use the advantages of the (Ti–B–Si–Ni)N coating with high hardness, but which would ensure the fulfillment, in the aggregate, of the above requirements – sufficient adhesion strength to the substrate, hardness and heat resistance. Based on the available literature data, we selected a coating composition which could be used for hard-alloy cutting tools and investigated its physical and mechanical properties. The chosen Ti–B–Si composition contained zirconium nitride and a combination of nitride-forming elements. This paper compares the results of investigations of the physical and mechanical properties of ZrN mononitride coating and (Zr + Ti–B–Si–Ni)N multicomponent coating that were performed before and after high-temperature annealing of the coating specimens in air.

MATERIALS AND METHODS

The ZrN and (Zr + Ti–B–Si)N coatings were produced by vacuum-arc deposition using E110 zirconium alloy (0.9–1.1% Nb) and pressed SHS cathodes. The SHS cathode was produced using an exothermic combination of Ti, B, and Si (2 : 2 : 1 in atomic proportion) with a Ni (10 at %) binder added to the initial powder composition [12]. The diameter of both types of cathodes was 80 mm. The coatings were deposited using a modernized NNV 6.6-I1 facility with two arc evaporators and hollow hot cathode plasma generator (PINK [14]) [15].

The substrates of the coating specimens were 8 mm diameter, 6 mm width of VK8 (WC + 8% Co) hard alloy, widely used in tool production. The specimens were pre-polished using Kemet diamond suspension to Ra ≈ 0.1 μm and, before being loaded into the vacuum chamber, were cleaned with gasoline in an ultrasonic bath and then rubbed with acetone. Then, two VK8 specimens were mounted on the turntable of the NNV 6.6-I1 facility with a special holder that rotated during the coating deposition process around its own axis and revolved relative to the arc evaporators and the gas plasma source. The rotation speed of the turntable was 3.5 rpm. The temperature of the specimen holder and, accordingly, the specimens themselves were measured with a THA thermocouple.

In all cases, at the first stage of the process, the specimens were cleaned and heated in argon (Ar) to 300°C using the PINK plasma source. Then they were further heated using an additional Zr-cathode arc evaporator to ensure the expected diffusion of the sputtered solid elements into the substrate surface layer and to enhance the adhesion of the substrate to the binding sublayer of the coating. This technology was chosen based on the diffusion model of the coating–substrate interface that predicts high values of the coating adhesion strength [16, 17]. The bias potential (*Ub*) was 900 V. The final temperature of the specimens after preliminary heating and their initial temperature at which the subsequent deposition of coatings assisted by the gas-discharge plasma was performed were both about 420°C. The binding Zr sublayers were deposited in argon at $Ub = 150$ V for the deposition time $t = 3$ min. The ZrN and (Zr + Ti–B–Si–Ni)N coating deposition was carried out by evaporation two cathodes of relevant composition at the same 150 V bias potential applied to the substrate but in an 90/10—N_2/Ar gas mixture. Our preliminary experiments have shown that the addition of argon to the flow of supplied nitrogen in the coating deposition scheme used provides a more stable discharge at the cathode (Ti–B–Si–Ni), but exceeding its addition by more than 10% reduces the probability of synthesizing stoichiometric zirconium nitride ZrN. In all cases, the arc discharge current was 60 A (minimized to reduce the proportion of the droplet component in the working material flow) for the zirconium cathodes and 80 A for the Ti–B–Si–Ni cathodes. The total pressure in the working chamber during the deposition of coatings was 0.6 Pa; the deposition time was 90 min. Thus, to perform comparative materials science investigations, coatings of two types were produced: ZrN (no. 1) and (Zr + Ti–B–Si–Ni)N (no. 2).

Initially, the thickness of the coating specimens was measured by the ball-cratering method (calo testing), and then their hardness was measured using a KBW1 hardness tester with a Vickers diamond pyramid at an indentation load of 0.1 N. The hardness was determined as the average of 10 measurements. All coating specimens were tested (each in three tests) for adhesion strength and brittleness by the Rockwell method at a load of 1500 N. The (Zr + Ti–B–Si–Ni)N coating specimens were additionally tested for adhesion strength by scratching them under increasing indentation load (scratch testing). This procedure was performed with a Revetest RST scratch tester (CSM Instruments, USA) using a Rockwell diamond cone indenter; simultaneously, the signal of acoustic emission (AE), depending on the indentation load, was recorded. The indentation load was increased linearly from 0 to 150 N. The optical image of the wear track of each (Zr + Ti–B–Si–Ni)N coating was obtained after scratch testing using a LeicaDMi8M inverted microscope (Leica Microsystems, Germany). The phase composition of coatings of both types was determined by X-ray phase analysis carried out with a Shimadzu XRD-7000S X-ray diffractometer using CuKα radiation. The phase composition was analyzed using the PDF 4+ database and the Crystallographica Search-Match code. The both types of coating specimens were additionally annealed in a SNOL muffle furnace in air at 700°C for 60 min. To simulate thermal shock conditions, they were unloaded from the furnace at 300°C and put on its massive steel base to ensure fast cooling. After this heat treatment, the coating hardness was measured again and X-ray phase analysis was performed using the above methods. It should be noted that such measurements could not be carried in out studies of (Ti–B–Si–Ni)N coatings [12] because of their complete delamination after annealing at 700°C.

Additionally, to investigate the heat resistance of the (Zr + Ti–B–Si–Ni)N coatings, a real-time X-ray phase analysis was performed using synchrotron radiation. This was done with the use of the VEPP-3 electron storage ring (BINP, SB, RAS) as a source of synchrotron radiation, an Anton Paar HTK-2000 high-temperature X-ray chamber, and an OD-3M-350 position-sensitive single-coordinate detector; the measurement data were processed using the Fityk v.1.3.1 code.

The characteristics of the synchrotron radiation were the following: operating wavelength 0.172 nm; temperature range from 30 to 1300°C in air; specimen heating rate 15°C/min; X-ray acquisition time 1 min per frame; diffraction angle range from 34 to 66°.

All X-ray diffraction patterns were reduced to the CuK_α radiation wavelength.

RESULTS AND DISCUSSION

Coating no. 1

On the average, the thickness of the ZrN coating was 3.3 μm, and its hardness HV was 31.5 GPa. In hardness tests, the penetration depth of the indenter into a coating specimen was no more than 0.1 of its thickness, which met the well-known standards for hardness measurements [18, 19]. The higher hardness of the ZrN coating, as compared with the reference data [20], might be due to the additional effect of the bombardment of the growing coating with the ions of the high-density gas-discharge plasma generated by the PINK source, namely, with an increase in the density of lattice defects and dislocations in the coating and with refinement of its structure [32].

Figure 1 shows an image of the typical Rockwell imprint on a specimen of this coating. As can be seen from this figure, the imprint has the shape of an inner circle, formed by the penetration of the diamond cone into the VK8 alloy substrate, which is surrounded by a ring enclosing the affected surface. As can be seen, there are neither a transition region between the black inner circle and the region of (possible) elastic-plastic deformation at the substrate–coating interface nor

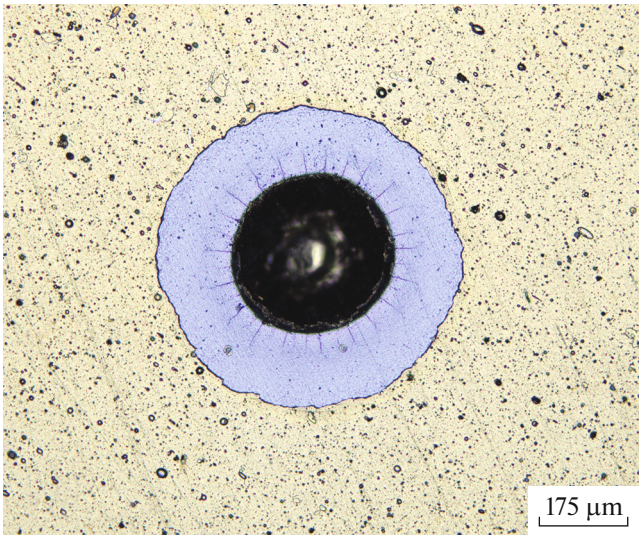

Fig. 1. Typical Rockwell imprint on a ZrN coating.

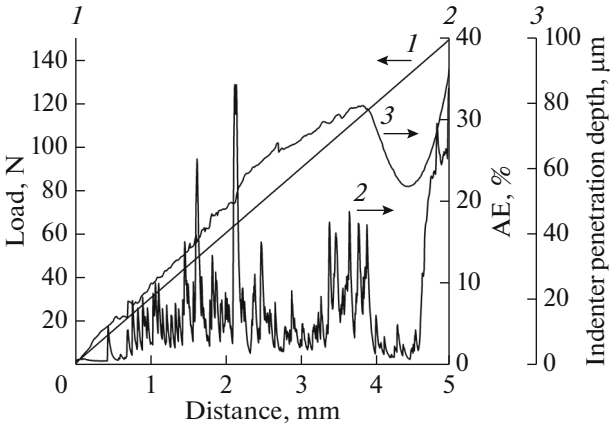

Fig. 2. The acoustic emission signal versus indenter load and depth of penetration into a ZrN coating.

visible traces of chipping and delamination of the coating.

Scratch-testing studies have shown the following. Already at low loads on the indenter (of the order of 10–20 N), a change in the linear nature of the depth of its penetration from the load and the appearance of pronounced acoustic emission signals are observed (Fig. 2). The increase in AE signal amplitudes observed when the indenter moves along the wear track at a distance of about 1 mm or more is presumably due to elastic-deformation effects in the process of its interaction with the coating material, which is confirmed by the appearance of peculiar "rollers" on this track (Fig. 3). At a distance of more than 1.5 mm, the beginning of delamination of the coating along the periphery of the scratch track and a sharp jump in the AE signal are observed.

After high-temperature annealing of this coating, its hardness *HV* was 5.8 GPa, and X-ray phase analysis showed, along with the presence of tungsten trioxide, a residual content of ZrN zirconium nitride (Fig. 4).

Coating no. 2

The thickness of the (Zr + Ti–B–Si–Ni)N multicomponent coating was 3.9 μm, and its hardness *HV* was 40.9 GPa in the initial state and 9.1 GPa after high-temperature annealing. The values of these parameters are superior of the values obtained for the ZrN coating. The higher hardness of this coating could be not only due to the assisted ion bombardment from the PINK source, but also due to its multilayer structure that was formed when the specimens passed through the evaporation zones of cathodes of different compositions. This is indirectly evidenced by the clear difference between the region of the transition from the black inner circle to the periphery of the coating on the Rockwell imprint image (Fig. 5) from the similar region on the ZrN coating having a zone with clear signs of elastic-plastic deformation.

In previous works, with the participation of the authors of presented article and according to a similar scheme of vacuum-arc plasma-assisted deposition of CrN/ZrN coatings by evaporation of cathodes two different compositions, the microlayer nature of coatings with layers of the nanoscale range was convincingly confirmed by the Transmission electron microscopy method [7].

For this coating, to additionally evaluate its adhesion strength, scratch testing was performed. Figure 6 and show the typical dependence of the acoustic emission (AE) signal on the load and depth of penetration of the indenter and the corresponding image of the wear track obtained during this test.

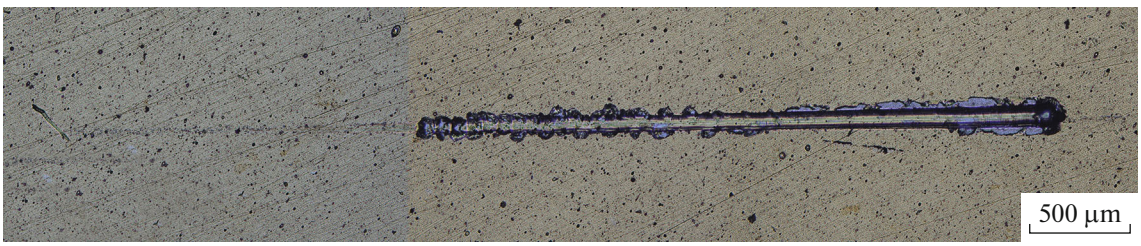

Fig. 3. Image of the wear track on a ZrN coating after scratch testing.

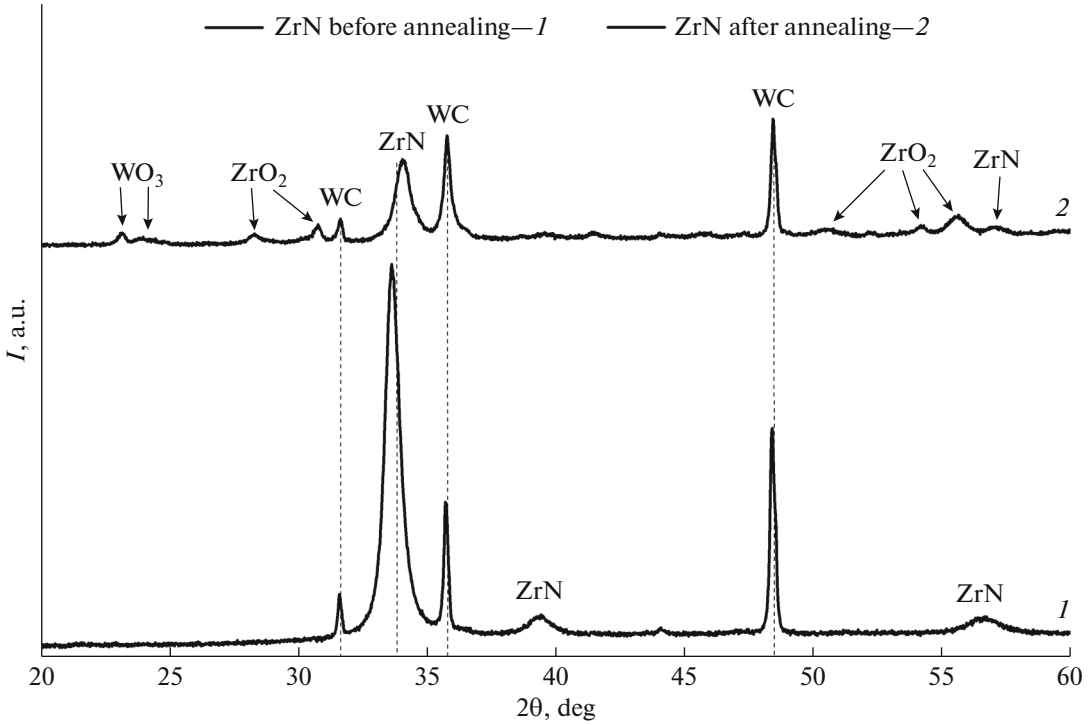

Fig. 4. Data of X-ray phase analysis of a ZrN coating before (lower curve) and after annealing at 700°C for 60 min (upper curve).

The linear behavior of the depth of penetration of the indenter into the surface was retained up to a load of about 120 N. In this case, the penetration depth was evidently larger than the coating thickness, which was also observed in the previous experiment [27]. At a distance of about 1.5 mm from the beginning of the indenter path, bursts of AE signals began to be recorded, although the coating had not yet worn out. This is evidence that the indentation induced elastic deformation the coating material (Fig. 7). These indicators exceed those of the ZrN coating (Figs. 2 and 3) and indicate a high adhesion strength of the (Zr + Ti–B–Si–Ni)N coating to the substrate.

X-ray phase analysis of a (Zr + Ti–B–Si–Ni)N coating specimen performed before annealing showed the presence of zirconium nitride, titanium nitride, and titanium boride (Fig. 8). The same analysis performed after annealing of this specimen detected zirconium oxide along with preserved zirconium nitride

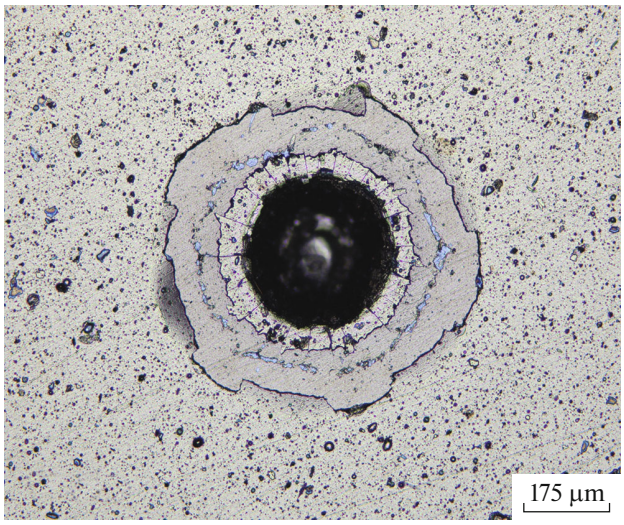

Fig. 5. Typical Rockwell imprint on a (Zr + Ti–B–Si–Ni)N coating.

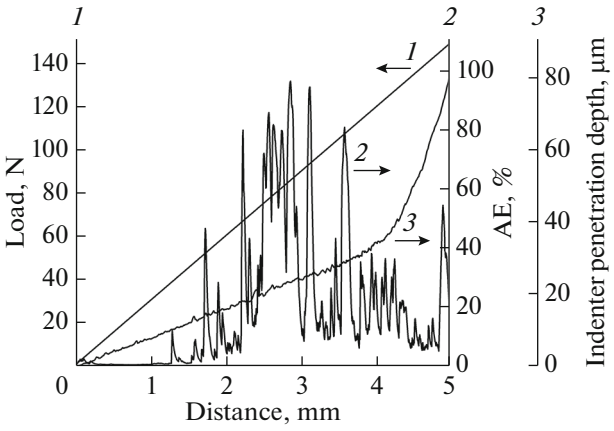

Fig. 6. The acoustic emission signal versus indenter load and depth of penetration into a (Zr + Ti–B–Si–Ni)N coating.

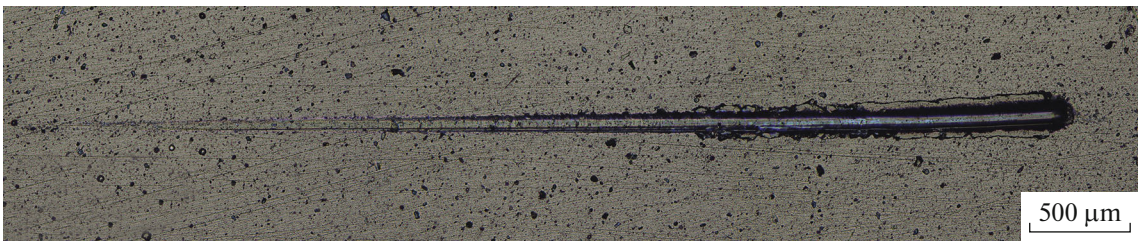

Fig. 7. Image of the wear track on a(Zr + Ti–B–Si–Ni)N coating after scratch testing.

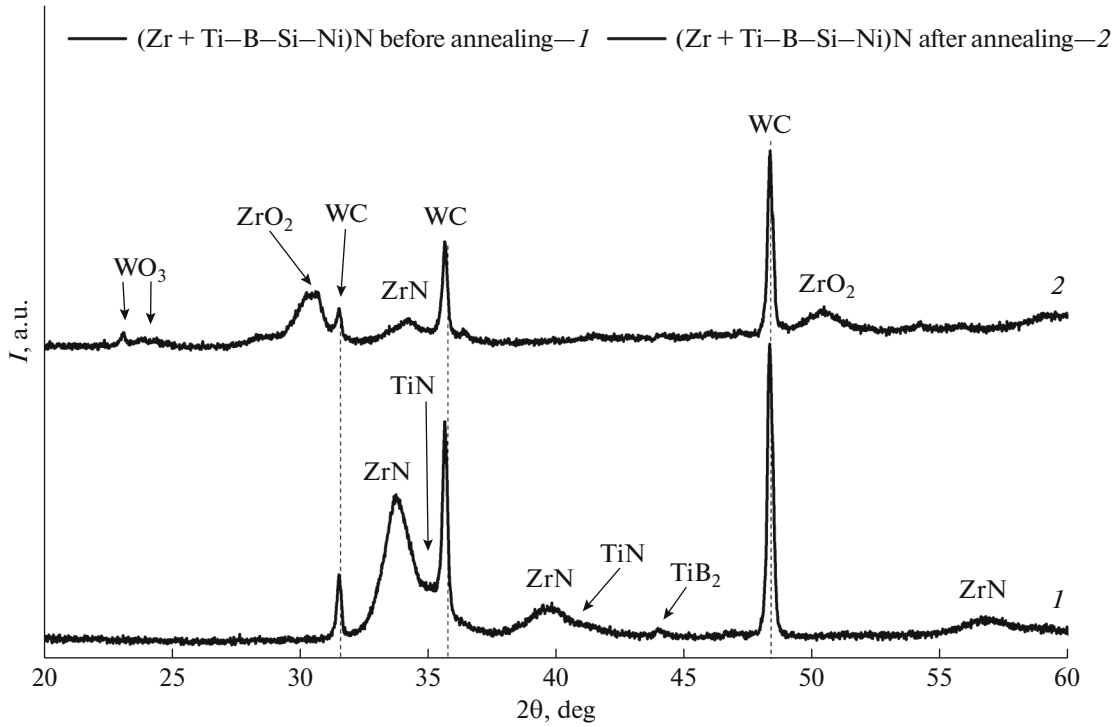

Fig. 8. Data of X-ray phase analysis of a (Zr + Ti–B–Si–Ni)N coating specimen obtained before (lower curve) and after annealing at 700°C for 60 min (upper curve).

(Fig. 8). The recorded presence of titanium borides in the initial state of the (Zr + Ti–B–Si–Ni)N coating, in comparison with the ZrN coating, can serve, in addition to its microlayering, as an additional factor in the increase in hardness.

The resistance of the (Zr + Ti–B–Si–Ni)N coating to high-temperature oxidation and the stability of its structure and phase state were investigated by the method of X-ray phase analysis using synchrotron radiation in the temperature range from 30 to 1170°C in air.

It was observed that when a specimen of the coating was heated in air, its structure was stable up to a temperature of ~700°C (Fig. 9). Above this temperature, the structure and phases of the coating were rearranged, which manifested in the disappearance of reflections of zirconium nitride (ZrN) at refraction angles around 40° and 57° and the appearance of a broad reflection of zirconium oxide (ZrO_2) at an angle around 50°. The observed structure and phase rearrangement were consistent with the data of X-ray phase analysis obtained for the (Zr + Ti–B–Si–Ni)N coating after annealing at 700°C (Fig. 8). Thereafter, at a temperature of ~1030°C, intense oxidation of the coating material began, broad reflections of zirconium nitride (at ~34°) and zirconium oxide (at ~50°) disappeared, and a group of weak narrow reflections appears. At a temperature of ~1140°C, the specimen was destroyed; as a result, the diffracting surface left the field of view of the diffractometer optics and all coating reflections disappeared. Starting from a temperature of ~1170°C, the specimen was cooled at a rate of 100° C/min to room temperature. A series of X-ray diffraction patterns obtained during heating and cooling of the specimen is shown in Fig. 9.

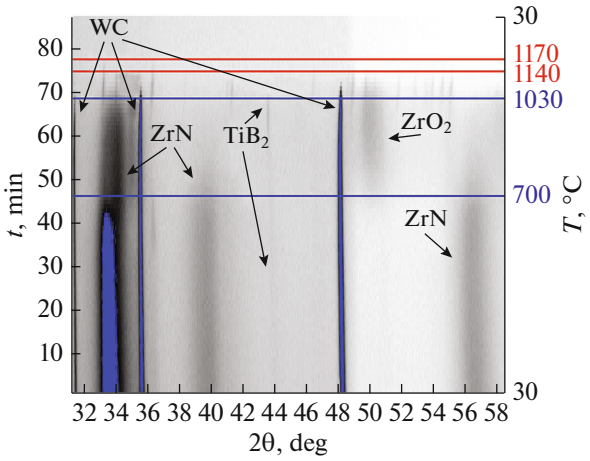

Fig. 9. X-ray diffraction patterns of a (Zr + Ti–B–Si–Ni)N coating deposited on a VK8 alloy substrate, obtained when the specimen was heated in air to 1170°C and then cooled to 30°C.

CONCLUSIONS

(1) Pressed Ti–B–Si–Ni SHS cathodes were tested and the technological capabilities of them for the vacuum-arc synthesis of multicomponent coatings with a zirconium cathode were confirmed.

(2) It has been experimentally demonstrated that simultaneous sputtering of these cathodes carried out sequentially makes it possible to produce (Zr + Ti–B–Si–Ni)N multicomponent coating of hardness at least 40 GPa showing good adhesion to a (WC + Co) hard alloy substrate and retaining a relatively high hardness (9.1 GPa compared to 5.8 GPa for ZrN) after annealing in air at 700°C.

(3) X-ray phase analysis performed using synchrotron radiation generated by the VEPP-3 electron storage ring (BINP, SB, RAS) has confirmed quite high resistance of the (Zr + Ti–B–Si–Ni)N coating to high-temperature oxidation.

(4) The results of mechanical and physical investigations allow the conclusion that the properties of the (Zr + Ti–B–Si–Ni)N multicomponent coating are optimally combined and, in general, exceed those of the ZrN mononitride coating.

(5) The developed multicomponent coating can be used to improve the wear resistance of carbide cutting tools instead of the traditional ZrN mononitride coating.

FUNDING

The deposition of coatings and the investigations of their physical and mechanical properties were carried out within the framework of the state assignment of the Ministry of Science and Higher Education of the Russian Federation on topic no. FWRM-2022-0001. The investigations of the coating phase composition and resistance to high-temperature oxidation performed by the method of X-ray phase analysis using synchrotron radiation were supported by the Ministry of Science and Higher Education of the Russian Federation (project no. 075-15-2021-1348) as part of event no. 3.1.18.

CONFLICT OF INTEREST

The authors of this work declare that they have no conflicts of interest.

REFERENCES

1. I. Konyashin, G. Fox-Rabinovich, and A. Dodonov, J. Mater. Sci. **32**, 6029 (1997). https://doi.org/10.1023/A:1018679414707
2. H. M. Gabriel and K. H. Kloos, Thin Solid Films **118**, 243 (1984). https://doi.org/10.1016/0040-6090(84)90195-0
3. W. J. Chou, G. P. Yu, and J. H. Huang, Surf. Coat. Technol. **149**, 7 (2002). https://doi.org/10.1016/S0257-8972(01)01382-2
4. W. J. Chou, G. P. Yu, and J. H. Huang, Surf. Coat. Technol. **167**, 59 (2003). https://doi.org/10.1016/S0257-8972(02)00882-4
5. Y. C. Chieh, W. Z. Lo, and F. H. Lu, Surf. Coat. Technol. **200**, 3336 (2006). https://doi.org/10.1016/j.surfcoat.2005.07.048
6. H. M. Benia, M. Guemmaz, G. Schmerber, A. Mosser, and J. C. Parlebas, Appl. Surf. Sci. **200**, 231 (2002). https://doi.org/10.1016/S0169-4332(02)00925-X
7. A. Vorontsov, A. Filippov, N. Shamarin, E. Moskvichev, O. Novitskaya, E. Knyazhev, Y. Denisova, A. Leonov, V. Denisov, and S. Tarasov, Metals **12**, 1746 (2022). https://doi.org/10.3390/met12101746
8. V. P. Tabakov and A. V. Chikhranov, Stanki Instrum. **7**, 17 (2009).
9. V. M. Beresnev, O. V. Sobol, S. S. Grankin, U. S. Nemchenko, V. Yu. Novikov, O. V. Bondar, K. O. Belov, O. V. Maksakova, and D. K. Eskermesov, Inorg. Mater.: Appl. Res. **7**, 388 (2016). https://doi.org/10.1134/S2075113316030047
10. S. I. Altukhov, A. A. Yermoshkin, K. S. Smetanin, A. F. Fedotov, V. N. Lavro, Ye. I. Latukhin, and A. P. Amosov, Izv. Samar. Nauchn. Tsentra Ross. Akad. Nauk **13**, 77 (2011).
11. S. I. Altukhov, A. P. Amosov, A. N. Asmolov, V. I. Bogdanovich, A. A. Yermoshkin, D. A. Zakharov, V. G. Krutsilo, Ye. I. Latukhin, and A. F. Fedotov, Izv. Samar. Nauchn. Tsentra Ross. Akad. Nauk **15**, 568 (2013).
12. V. M. Savostikov, A. A. Leonov, V. V. Denisov, Yu. A. Denisova, A. B. Skosyrskiy, and I. A. Shulepov, J. Surf. Invest.: X-ray, Synchrotron Neutron Tech. **17**, 686 (2023). https://doi.org/10.1134/S102745102303031X
13. A. A. Vereshchaka, Vestn. Bryansk. Gos. Tekh. Univ. **4** (48), 25 (2015). https://doi.org/10.12737/17077
14. V. N. Devyatkov, Y. F. Ivanov, O. V. Krysina, N. N. Koval, E. A. Petrikova, and V. V. Shugurov, Vacuum **143**, 464

(2017).
https://doi.org/10.1016/j.vacuum.2017.04.016

15. A. A. Leonov, Y. A. Denisova, V. V. Denisov, M. S. Syrtanov, A. N. Shmakov, V. M. Savostikov, A. D. Teresov, Coatings **13**, 351 (2023). https://doi.org/10.3390/coatings13020351
16. P. A. Topolyanskiy, S. A. Yermakov, and A. P. Topolyanskiy, Voronezh. Nauchno-Tekh. Vestn. **3**, 11 (2021). https://doi.org/10.34220/2311-8873-2022-11-27
17. M. G. Hocking, V. Vasantasree, and P. S. Sidky, *Metallic and Ceramic Coatings: Production, High Temperature Properties and Applications* (Longman, London, 1989; Mir, Moscow, 2000).
18. N. Panich and Y. Sun, Surf. Coat. Technol. **182**, 342 (2004). https://doi.org/10.1016/j.surfcoat.2003.07.002
19. Y. Sun, T. Bell, and S. Zheng, Thin Solid Films **258**, 198 (1995). https://doi.org/10.1016/0040-6090(94)06357-5
20. G. V. Samsonov and I. M. Vinitskiy, *Refractory Compounds: Handbook*, 2nd ed. (Metallurgiya, Moskva, 1976) [in Russian].
21. S. Veprek, M. Veprek-Heijman, P. Karvankova, and J. Prochazka, Thin Solid Films **476**, 1 (2005). https://doi.org/10.1016/j.tsf.2004.10.053